ATM is a cytoplasmic protein in mouse brain required to prevent lysosomal accumulation

Carrolee Barlow*[†‡], Catherine Ribaut-Barassin[§¶], Theresa A. Zwingman[¶‖], Amber J. Pope[†¶], Kevin D. Brown[¶**], Jennie W. Owens[††], Denise Larson[†], Elizabeth A. Harrington[‡‡], Anne-Marie Haeberle[§], Jean Mariani[§§], Michael Eckhaus[††], Karl Herrup[‖], Yannick Bailly[§], and Anthony Wynshaw-Boris[†¶¶]

*The Salk Institute for Biological Studies, Laboratory of Genetics, 10010 North Torrey Pines Road, La Jolla, CA 92037; [†]Genetic Disease Research Branch, National Human Genome Research Institute, Bethesda, MD 20892; [§]Laboratoire de Neurobiologie Cellulaire, Unité Propre de Recherche 9009 Centre National de la Recherche Scientifique, Centre de Neurochimie, 5 Rue Blaise Pascal, 67084 Strasbourg, France; [‖]Department of Neurosciences and Alzheimer Research Laboratory, Case Western Reserve University School of Medicine, 10900 Euclid Avenue, Cleveland, OH 44106; **Department of Biochemistry and Molecular Biology and The Stanley S. Scott Cancer Center, Louisiana State University Medical Center, New Orleans, LA 70112; [††]Veterinary Resources Program, Office of Research Services, Bethesda, MD 20892; [‡‡]Laboratory of Molecular Oncology, Massachusetts General Hospital Cancer Center, Charlestown, MA 01029; and [§§]Laboratoire Développement et Vieillissement du Système Nerveux, Unité Mixte de Recherche 7624 Centre National de la Recherche Scientifique, Université Pierre and Marie Curie, Boite 14, 9 quai Saint Bernard, 75005 Paris, France

Edited by David Baltimore, California Institute of Technology, Pasadena, CA, and approved November 9, 1999 (received for review June 9, 1999)

We previously generated a mouse model with a mutation in the murine *Atm* gene that recapitulates many aspects of the childhood neurodegenerative disease ataxia-telangiectasia. *Atm*-deficient (*Atm*−/−) mice show neurological defects detected by motor function tests including the rota-rod, open-field tests and hind-paw footprint analysis. However, no gross histological abnormalities have been observed consistently in the cerebellum of any line of *Atm*−/− mice analyzed in most laboratories. Therefore, it may be that the neurologic dysfunction found in these animals is associated with predegenerative lesions. We performed a detailed analysis of the cerebellar morphology in two independently generated lines of *Atm*−/− mice to determine whether there was evidence of neuronal abnormality. We found a significant increase in the number of lysosomes in *Atm*−/− mice in the absence of any detectable signs of neuronal degeneration or other ultrastructural anomalies. In addition, we found that the ATM protein is predominantly cytoplasmic in Purkinje cells and other neurons, in contrast to the nuclear localization of ATM protein observed in cultured cells. The cytoplasmic localization of ATM in Purkinje cells is similar to that found in human cerebellum. These findings suggest that ATM may be important as a cytoplasmic protein in neurons and that its absence leads to abnormalities of cytoplasmic organelles reflected as an increase in lysosomal numbers.

ATM is one of a growing family of conserved high-molecular-mass kinases with homology to protein and lipid kinases. This family is known to regulate diverse processes such as mitotic checkpoints, meiosis, telomere length monitoring, and V(D)J recombination in organisms from yeast to mammals. ATM is a large phosphoprotein that is ubiquitously expressed. Studies have shown that ATM is present predominantly within the nucleus of cultured human cells with a small fraction present in the cytoplasm (1–3). Work with cell lines from patients with ataxia-telangiectasia (A-T) and *in vivo* and *in vitro* studies with cells and tissues from *Atm*−/− mice have identified defects in molecular pathways that are normally activated after DNA double-strand breaks in the genome (for reviews, see refs. 4 and 5). It is likely that ATM participates in initiating signal transduction pathways via its kinase activity to regulate the activity of molecules that manage cell-cycle arrest and repair. Therefore, ATM deficiency predictably results in radiosensitivity, germ cell degeneration, mild immunodeficiency, and an extreme sensitivity to developing T cell lymphomas.

Whereas the DNA damage response function of ATM is well documented, no clear understanding of its function in postmitotic cells has been established. This lack of understanding is particularly poignant in that neurodegeneration of postmitotic neurons is the hallmark manifestation of A-T in humans. Although *Atm*−/− mice faithfully recapitulate the human disorder in many respects, a general lack of neuronal degeneration has been reported by several groups when animals have been examined at a young age before tumor formation (6–9). However, one group reported neuronal degeneration detectable by electron microscopy (EM; ref. 10).

We performed an analysis of cerebellum from young, tumor-free *Atm*−/− mice to determine whether neuronal abnormalities exist and to identify anatomical lesions that may help explain the neurological dysfunction. Our study also examined the cellular localization of the ATM protein in the adult nervous system.

Materials and Methods

Generation and Use of *Atm*−/− Mice. *Atm*−/− mice were generated as described (6). Animals were either inbred 129SvEv or Black Swiss/129SvEv backgrounds. No significant strain differences were found with the exception of a similarly increased incidence of ectopic Purkinje cells (PCs) in both *Atm*−/− and wild-type mice of the 129SvEv background (data not shown). *Atm*−/− and control mice used in one EM study were generated independently, maintained in an outbred background, and kindly provided by David Baltimore and Yang Xu (California Institute of Technology; ref. 9). Animals were 4–16 weeks of age. Because all lines of *Atm*−/− mice show a near complete penetrance of T cell lymphoma formation beginning at 10–12 weeks of age, we used two methods to ensure that lymphomas did not contribute to any findings. The majority of animals used were 4–12 weeks of age, a time when most animals remain tumor-free. All animals were carefully examined for the presence of T cell lymphomas by using gross and microscopic inspections. Any animal with evidence of tumor was excluded from the analysis. Animal procedures were performed according to protocols approved by The Salk Institute for Biological Studies and the National Institutes of Health animal care and use committees.

Antibody Production and Immunoblotting. BALB/c mice were immunized with a bacterially produced, purified His-tagged fusion protein encoding amino acids 2,165–2,715 of human ATM to generate the monoclonal antibody AM9. After a 3-month

This paper was submitted directly (Track II) to the PNAS office.

Abbreviations: A-T, ataxia telangiectasia; EM, electron microscopy; PC, Purkinje cell.

[‡]To whom reprint requests should be addressed. E-mail: barlow@salk.edu.

[¶]C.R.-B., T.A.Z., A.J.P., and K.D.B. contributed equally to this work.

[¶¶]Present address: Departments of Pediatrics and Medicine, University of California, San Diego, CA 92093.

The publication costs of this article were defrayed in part by page charge payment. This article must therefore be hereby marked "*advertisement*" in accordance with 18 U.S.C. §1734 solely to indicate this fact.

immunization schedule, mouse splenocytes were fused with SP2/0 myeloma cells, and resultant hybridomas were isolated (11). Characterization of anti-ATM monoclonal antibody specificity was done by immunoblotting and immunoprecipitation assays (E.A.H. and K.B., unpublished work). Immunoblotting was performed as described (1, 12). Indicated loads of protein were electrophoresed on 7.5% low crosslinking acrylamide gels (121:1 acrylamide:bisacrylamide). After electrophoresis and electrotransfer, the blots were incubated in spent AM9 tissue culture supernatant at a dilution of 1:2. Immunoblot signals were detected by using a chemiluminescent protocol (Supersignal, Pierce) and recorded on Kodak x-ray film.

Immunohistochemistry. Mice were anesthetized with an intraperitoneal avertin injection (80 μg per g body weight) prepared by dissolving 2.5 g of 2,2,2-tribromoethanol in 5 ml of *tert*-amyl alcohol (Aldrich Chem, Metuchen, NJ) at 37°C for 30 min. The rib cage was reflected to expose the heart; the lower left ventricle was cannulated; and saline/heparin solution (0.1 M Sorensen's buffer, pH 7.4/10 units/ml heparin) was circulated, followed by fresh 4% (vol/vol) paraformaldehyde. The right atrium was cut to allow outflow of the blood and perfusion solutions. Tissues were either sectioned after paraffin embedding or cryoprotected overnight in 20% (vol/vol) sucrose, mounted in OCT media, and cut at −20°C in a cryostat. Paraffin sections were deparaffinized, and immunohistochemistry was performed by using ABC reagents, secondary antibodies, and detection (Vector Laboratories) according to standard protocols. AM9 was used undiluted or diluted 1:5 in all tissues, with *Atm*−/− mouse tissues used as controls for nonspecific binding.

PC Counts. PCs were counted by using previously described profile-based counting methods (13). Animals were perfused with 4% (vol/vol) paraformaldehyde in 0.1 M phosphate buffer. The brain was excised from the skull case and stored overnight in fresh fixative. The next day, the tissue was dehydrated through graded alcohol and infiltrated with paraffin (Paraplast Plus, Fisher). By using standard histological methods, a full set of serial 10-μm sections was collected for each half cerebellum counted. Every 20th section was stained with 0.2% Cresyl violet and examined at ×40. PCs were identified by their large size and position in the PC layer.

Golgi–Cox Staining and Analysis. Animals were euthanized by carbon dioxide asphyxiation; brains were removed and immersed in fixative (10 mg/ml potassium dichromate/10 mg/ml mercuric chloride/4.5 mg/ml potassium chromate; precipitate was cleared with 0.1 M HCl). Brains were stored in the dark undisturbed for 6–8 weeks. Tissue was dehydrated first in equal parts acetone and alcohol at room temperature for 24 h. Solution was replaced with ether alcohol (anhydrous ether/ethyl alcohol) for 24 h at room temperature. Brains were then infiltrated with low-viscosity nitrocellulose celloidin/parlodion (Fisher) at a concentration of 5% (vol/vol; 2 days), 10% (vol/vol; 1 day), and 12% (vol/vol; 5 days). Brains were embedded in fresh 12% (vol/vol) low-viscosity nitrocellulose and hardened with chloroform vapors overnight. Blocks were stored in 70% (vol/vol) EtOH until cut with a sliding microtome, and 100-μm sections were hydrated in distilled water for 15 min and developed in 5% (vol/vol) sodium sulfite for 20 min. Sections were dehydrated in 95% (vol/vol) ethanol for 1 h, cleared in terpineol overnight, and mounted and coverslipped with Permount.

EM. Animals were prepared by using three methods. One set of animals was perfused transcardially (80–101 mmHg; 1 mmHg = 133 kPa) with 500 ml of 1% glutaraldehyde/1% formaldehyde/0.1 mM $CaCl_2$ in 0.12 M sodium potassium phosphate buffer (pH 7.25). Heads were kept at 4°C for 2 h before the cerebrum and cerebellum were excised and postfixed for at least 18 h at 4°C. Samples were punched in 5-μm-thick nonadjacent vibratome sections cut sagittally in the hippocampus and in the vermal cortex and fastigial nucleus of the cerebellum (two samples per region per section in five sections per mouse). The samples were fixed secondarily for 3 h in 2% (vol/vol) osmium tetroxide in phosphate buffer and counterstained in 2.5% (vol/vol) uranyl acetate before being processed for dehydration and embedding in Araldite (Fluka). Random sections were prepared by using a Reichert–Jung ultracut-E ultramicrotome. In a separate experiment, mice were perfused with 2.5% (vol/vol) glutaraldehyde/2% (vol/vol) formaldehyde/6% (vol/vol) sucrose in 0.1 M Sorensen's buffer (pH 7.4) for 8 min. After perfusion, samples of cerebellum and hippocampus were fixed by immersion in 2.5% (vol/vol) glutaraldehyde/2% (vol/vol) formaldehyde/6% (vol/vol) sucrose in 0.1 M Sorensen's buffer (pH 7.4) and then postfixed in 1% osmium tetroxide. Tissues were dehydrated through alcohol and propylene oxide and embedded in Eponate 12 resin (Ted Pella, Redding, CA). Random thin sections were prepared with a Sorvall MT-2B ultramicrotome and stained with uranyl acetate and lead citrate. Finally, in a third experiment, mice were perfused by using 2.5% (vol/vol) glutaraldehyde/2% (vol/vol) formaldehyde/0.5 M sucrose in O.1 M cacodylate buffer (pH 7.2) for 10 min. After perfusion, samples were fixed for an additional 1.5 h at room temperature by immersion in 0.1 M cacodylate buffer (pH 7.2). Samples were postfixed in 1% osmium tetroxide in PBS/0.05 M sucrose for 1 h at room temperature, rinsed in water three times for 15 min, and processed for 1 h in 0.5% uranyl acetate at room temperature. Tissues were dehydrated with acetone and embedded in Spurr's resin (Electron Microscopy Sciences, Fort Washington, PA). Random thin sections were prepared with a Reichert–Jung ultracut-E ultramicrotome and stained with lead citrate.

Sections were examined by using a Philips Electronic Instruments (Mahwah, NJ) 201 or EM420 (80-kV) EM, a Siemens (Iselin, NY) Elmiskop 101 (60-kV) EM, or a JEOL 100CX EM. Examination and analysis were performed in three separate laboratories in a blinded fashion. In one laboratory, 1 mm^2 per block was examined by using 10 blocks per region per mouse such that 10 mm^2 per mouse was viewed for a total analysis of 50 mm^2 of cerebellar cortex from five wild-type and five *Atm*−/− mice. Similar analyses were performed independently in two other laboratories with a total of four controls and four *Atm*−/− mice.

Lysosomal Counts. Ultrathin sections were cut (one level ≈ 10 sections per block) from two to four randomly chosen blocks per mouse. Grids were examined under EM, and the total number of lysosomes per grid and total number of PCs per grid were counted in a blinded fashion. Each grid was independently counted by two persons per laboratory. The somatic neuroplasm of 94 PCs from five wild-type mice and of 120 PCs from five *Atm*−/− mice as well as the neighboring molecular and granular layers were photographed. Areas of the cell cytoplasm ranged from 88 to 100 μm^2 per cell in the wild-type mice and from 88 to 96 μm^2 per cell in the *Atm*−/− mice. All types of membrane-bound lysosomes larger than 0.1 μm were identified morphologically and counted; these included primary and secondary lysosomes and lipofuscin-containing lysosomes. Vacuoles, multivesicular and fibrillary bodies, as well as degraded mitochondria and membranes were discarded from the counts. However, no increase in multivesicular bodies was found. The lysosomes of glial cell processes, dendrites, axons, and non-PC neurons were not counted.

Results and Discussion

ATM Is Localized to the Cytoplasm of PCs and a Subset of Dorsal Root Ganglia Neurons. Western blotting of extracts from wild-type and *Atm*−/− mouse brain showed that AM9 antibody recognized

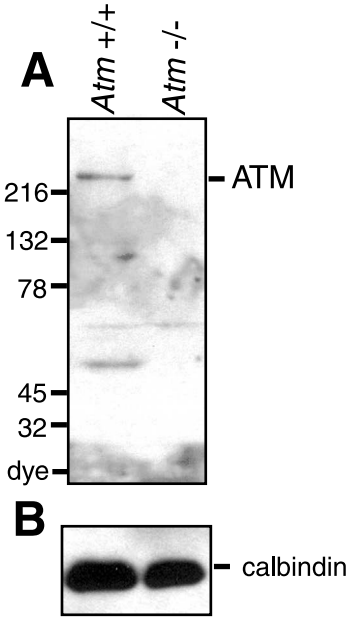

Fig. 1. ATM is expressed in adult brain. (*A*) Protein (100 μg) obtained from SDS extracts of wild-type (lane 1) and *Atm*−/− mouse (lane 2) cerebella was subjected to electrophoresis on a 5–15% linear acrylamide gradient gel, followed by immunoblotting with AM9. Note reactivity with the high-molecular-mass (≈350 kDa) ATM protein. Additional immunoreactivity was observed against a ≈55-kDa protein that is likely to be a proteolytic fragment of ATM, because its presence is confined to the extract from wild-type brain. (*B*) Extracts used in *A* (5 μg) were subjected to analysis with a calbindin antibody (Chemicon) to confirm equal protein loading.

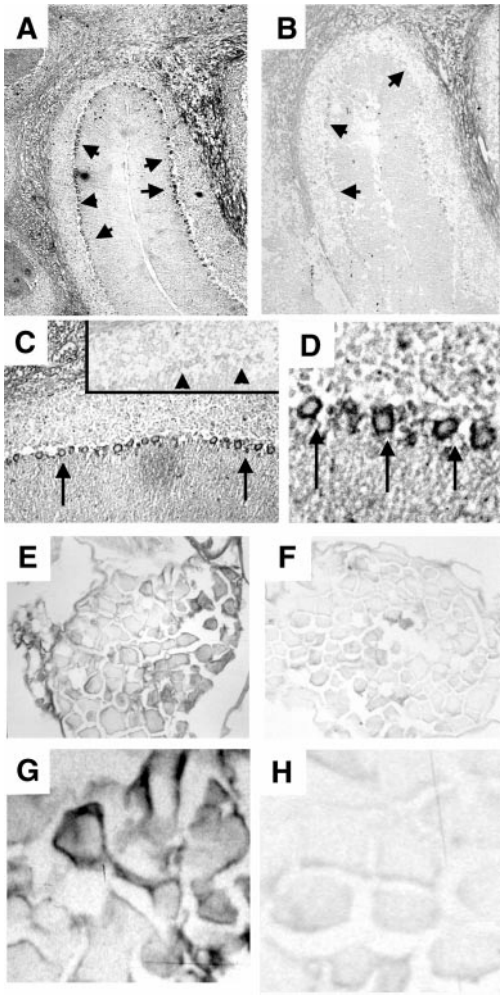

Fig. 2. ATM is present in the cytoplasm of adult PCs and dorsal root ganglia neurons. Detection of cytoplasmic ATM immunoreactivity in the cerebellum from a wild-type mouse in the PC layer (arrows) (magnification: *A*, ×10; *C*, ×40; *D*, ×100) and lack of staining in the *Atm*−/− mouse [magnification: *B*, ×10 (see arrows); *C Inset*, ×40 (see arrowheads)]. (*E* and *G*) ATM cytoplasmic immunoreactivity in the wild-type dorsal root ganglia (magnification: *E*, ×10; *G*, ×100). (*F* and *H*) No specific signal is detected in the *Atm*−/− mouse (magnification: *F*, ×10; *H*, ×100). (Bar = 0.5 μm.)

ATM (Fig. 1). The antibody staining indicated that ATM is expressed in wild-type adult cerebellum but is absent in *Atm*−/− cerebellum. *Atm*−/− mouse tissues were used as a negative control for all immunohistochemical experiments with this antibody to study the localization of ATM in tissue sections. We focused on the cerebellum and dorsal root ganglia, because the cerebellum is affected early in the disease and because high levels of RNA expression have been found in adult mouse dorsal root ganglia (14). ATM immunostaining localized to the PC layer of the cerebellar cortex (Fig. 2*A*). At higher magnification, the protein appears exclusively cytoplasmic in the PCs (Fig. 2 *C* and *D*). No staining was detected in the control *Atm*−/− mouse brain (Fig. 2*B*). Interestingly, the pattern of localization of ATM in mouse cerebellum is similar to that in human adult cerebellum reported recently (15). Likewise, cytoplasmic ATM immunoreactivity was present in a subset of neurons in the dorsal root ganglia in the wild-type mouse (Fig. 2 *E* and *G*), and no specific staining was observed in the *Atm*−/− mouse (Fig. 2*F* and *H*). We were unable to detect ATM in other brain regions by using this antibody.

The predominantly cytoplasmic localization of ATM in these types of neurons is particularly intriguing. The catalytic domain of ATM has significant homology to that of the phosphatidylinositol-3 kinases, specifically the p110 catalytic subunit of phosphatidylinositol-3 kinase. These kinases are generally cytoplasmic proteins mediating signal transduction pathways in response to growth factor stimulation. Phosphatidylinositol-3 kinases play important roles in the cell including signaling to the nucleus, vesicle transport, and rearrangement of the cytoskeleton (16). Although ATM has not been shown to act as a lipid kinase, a fraction of ATM is found in the cytoplasm of mitotically active cells, and we have found that ATM is exclusively cytoplasmic in oocytes arrested in meiosis I (17). Recent evidence is consistent with a role for ATM in the cytoplasm, because it has been found to associate with β-adaptin, a cytoplasmic protein important for vesicle and protein transport (18). Furthermore, cells in which the protein is predominantly nuclear are competent to undergo cell division, as opposed to neurons, which are postmitotic, or oocytes, which are arrested in the cell cycle. It remains to be established whether the localization difference is due to tissue-specific functions of ATM or depends on the cell-cycle arrest imposed by the postmitotic nature of the cells.

***Atm*−/− Mice Have Normal Cerebellar Morphology.** We examined the cerebella of control and *Atm*−/− mice by using a combination of methods including stains for Nissl substance, parvalbumin, and calbindin immunohistochemistry. We found no significant differences in the morphology or distribution of neurons between wild-type and *Atm*−/− brain (data not shown). To obtain a more detailed picture of the morphology of dendritic arbors, we used Golgi–Cox staining. We examined three *Atm*−/− and three wild-type control littermates. We considered 130 PCs that were fully impregnated totally within the section and contained no breaks along the dendrites caused

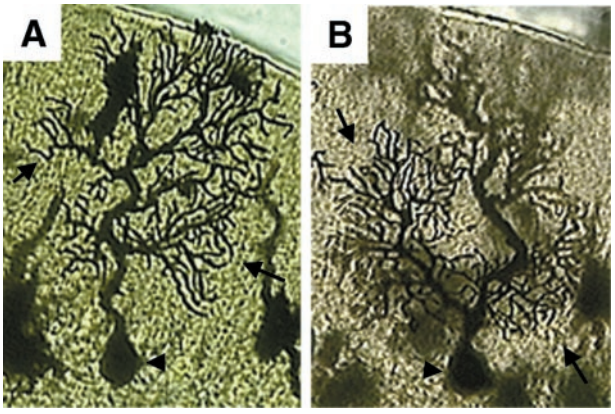

Fig. 3. Atm−/− mice have normal PC morphology. Golgi–Cox staining shows that the morphologies of PCs from adult cerebella from a wild-type (*A*) and an *Atm*−/− (*B*) mouse are similar. Note the normal morphology of the cell body (arrowhead) and extensive arborization of the dendritic tree (arrows) in both PCs, with no evidence of neurodegeneration.

by fixation or section artifacts. No abnormalities were detected in either the *Atm*−/− or wild-type samples (see Fig. 3 for an example). Finally, we performed terminal deoxynucleotidyl-transferase-mediated UTP end labeling to detect apoptosis, proliferating cell nuclear antigen staining to detect inappropriate cell-cycle activity, and flow cytometric and immunohistochemical analyses to analyze the number and character of microglia. We found a slight but statistically insignificant decrease in activated microglia and microglial numbers in *Atm*−/− mice, consistent with a relative immunodeficiency, and no other abnormalities (data not shown).

***Atm*−/− Mice Have Normal Numbers of PCs.** We also performed PC counts on two *Atm*−/− and two wild-type control animals. No obvious Purkinje-like cells were present in the molecular layer of either the mutant or the wild type. If there were PCs deep in the internal granule cell layer, these would have escaped detection, because they would have been mistaken for Golgi II cells. However, such a mistake was unlikely, because calbindin immunocytochemistry revealed no such cells in the sections we examined. Profile-based counting methods were used on 10-μm paraffin sections. All identified PCs that had a portion of the nucleus in the section were counted, and the areas under the curves were determined. The raw PC counts determined in this way differed by less than $\pm 3\%$ among the animals examined. Correcting for counting errors by the method of Hendry (19) did nothing to alter the result. These findings, in conjunction with neurological testing, indicate that neurologic dysfunction exists in young *Atm*−/− mice in the absence of anatomical defects detectable at the level of the light microscope.

***Atm*−/− Mice Have Increased Numbers of Lysosomes in PCs Detectable by EM but No Evidence of Neurodegeneration.** Although we were unable to show evidence of cerebellar morphology disruption or neurodegeneration, an isolated report suggested that one line of *Atm*−/− mice had evidence of neurodegeneration detectable by EM (10). Therefore, we performed EM analysis of cerebellum. We studied a total of five *Atm*−/− mice and five wild-type mice at 2.5–4 months of age. In addition, three *Atm*−/− and three control mice at greater than 4 months of age were studied (matched pairs of *Atm*−/− and control mice at 6, 8, and 12 months of age). We also conducted parallel studies on one wild-type and one *Atm*−/− mouse provided by D. Baltimore and Y. Xu (10), where neurodegeneration had been reported in three of the three animals analyzed.

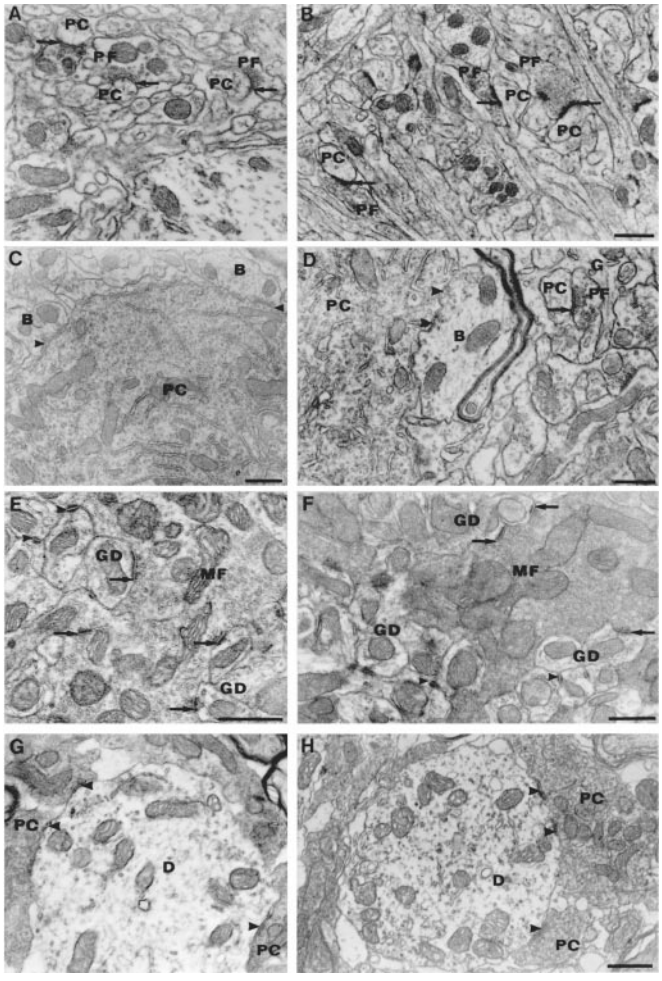

Fig. 4. The cerebella of wild-type and *Atm*−/− mice have analogous subcellular and synaptic ultrastructure. Asymmetric synapses (arrows) made by parallel fibers (PF) on PC spines in the molecular layer of wild-type (*A*) and *Atm*−/− (*B*) mice (magnification: ×24,000). (*C* and *D*) Symmetric synapses (arrowheads) made on PC soma by presumptive basket cell axon terminals (B) from wild-type (*C*) and *Atm*−/− (*D*) mice. A parallel fiber bouton (PF) with presynaptic vesicles makes an asymmetric synapse (arrow) on a postsynaptic dendritic PC spine in the deep molecular layer [glia (G); magnification: ×24,000]. (*E* and *F*) Glomerular synapses made by mossy fiber (MF) terminals (arrows) on granule cell dendrites (GD) in the internal granular layer of the wild-type (*E*) and *Atm*−/− (*F*) cerebellum. Arrowheads show tight junctions between GDs (magnification: *E*, ×36,000; *F*, ×27,000). (*G* and *H*) Synapses made by PC axon terminals (arrows) on the dendrites (D) of neurons in the fastigial nucleus of wild-type (*G*) and *Atm*−/− (*H*) cerebellum (magnification: ×27,000).

Qualitative evaluation of regions throughout the cerebellar cortex and the fastigial nucleus at the EM level did not disclose any significant difference between control and *Atm*−/− mice of all ages and strains (Fig. 4, compare *A*, *C*, *E*, and *G* with *B*, *D*, *F*, and *H*), suggestive of neurodegeneration. No degenerating PCs were found. The ultrastructural content of the soma and the dendrites of the neurons (PC, granule cells, and interneurons) appeared similar in all cases. Classical aspects of degeneration were rare in the neuropil of the molecular and granular layers of the *Atm*−/− mice as well as of the control mice. Axodendritic and axosomatic synapses of the asymmetric and symmetric types had normal structure and location throughout all layers of the cerebellar cortex of all mice examined. Therefore, there is no disorder detected in any area of the cerebellum suggestive of neurodegeneration, even at the level of the extracortical PC axon

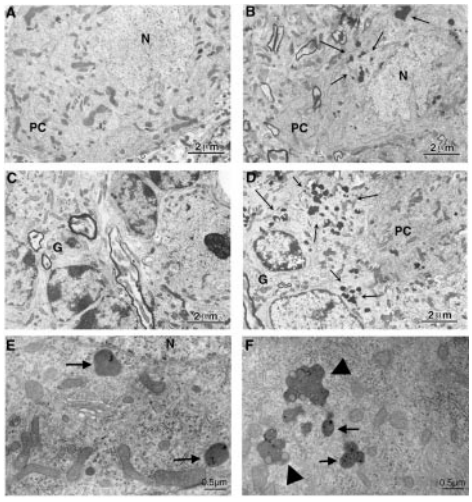

Fig. 5. Proliferation of somatic primary lysosomes and lipofuscin granules in the cerebellum of *Atm*−/− mice. Shown are PCs from a wild-type (*A*) mouse where lysosomes are rarely encountered. In contrast, in the *Atm*−/− PC shown, there are large clusters of lysosomes in the PC cytoplasm (*B*, arrows). Similar abnormalities could be seen outside of the PC layer. (*D*) Clusters of lysosomes in the granular cell layer (G) of the *Atm*−/− sample, which are not apparent in the control (*C*). (*E* and *F*) Detail of the fine structure of the lysosomes in the *Atm*−/− mouse brains. Somatic primary lysosomes are marked by arrows in *E*. lipofuscin granules (complex, engorged lysosomes; arrowheads) are shown in *F*. Note the lack of ultrastructural defects even in the presence of the lysosomal proliferation (n, neuropil; N, nucleus). Scale bars are as indicated.

terminals found in the deep cerebellar nuclei, such as the fastigial nucleus (Fig. 4 *G* and *H*).

Although we did not detect evidence of neurodegeneration, we found that the numbers of lysosomes (primary, secondary, and lipofuscin-containing lysosomes) in *Atm*−/− mice were increased in cerebellar PCs of all animals studied (Fig. 5). To quantify the increased frequency of lysosomes in the PC somata of the *Atm*−/− mice, we counted the lysosomes in size-matched neuroplasm areas of identical numbers of PC somata chosen randomly in control and *Atm*−/− mice (Table 1). We noted an approximate 2-fold increase in the number of lysosomes per PC. These experiments were extended to a few animals of other strains and ages including those provided by other investigators and older animals. Regardless of the strain or age, there was a consistent increase in lysosomes detected. However, the small number of older animals and animals from different strains analyzed precluded a statistical analysis in the older age group only. Of note, we observed a similar increase of lysosomal numbers in pyramidal cells of the hippocampus of mutant mice. Therefore, independent from the strain background, lysosomes have a tendency to proliferate or accumulate in PCs (and pyramidal neurons) in *Atm*−/− mice. Comparing the distribution of the lysosome numbers between *Atm*−/− and control PCs counted ($n = 55$ in each group) with the Kolmogorov–Smirnov test indicated that proliferation of lysosomes occurs in most *Atm*−/− PCs ($P < 0.05$). This finding rules out the possibility that ATM deficiency has differential lysosome-proliferating effect across the cell population.

The increase in lysosomes is likely an important finding, because abnormalities in lysosomes are considered a prominent morphologic marker of distressed neurons and because lysosomal abnormalities are associated with neurodegenerative diseases (20-24). Studies have suggested that accumulation of abnormal proteins, as in prion encephalopathies and formation of β/A4 protein from its precursor in Alzheimer's disease, takes place in lysosome-related organelles (24). Engorged lysosomes subsequently release their hydrolytic enzymes and are postulated actually to cause neuronal damage.

The abnormal increase in lysosomes in *Atm*−/− mice likely represents a primary event, because there is no evidence of neurodegeneration. The behavioral abnormalities of our mutant mice are consistent with neuronal compromise, and increased lysosomal numbers may represent an early abnormality in the disease process (1). It is interesting to note that several of the proposed functions of ATM, if lost, could manifest as lysosomal proliferation and/or dysfunction. For example, ATM is homologous to the phosphatidylinositol-3 kinase family of lipid kinases. Phosphoinositide signaling is involved in vesicle docking/fusion, as well as other membrane transport reactions along the lysosomal sorting pathways (16). In addition, it was recently shown that ATM interacts with β-adaptin, a component of the AP-2 adaptor complex that is involved in clathrin-mediated endocytosis. Therefore, in the absence of ATM, intracellular vesicle and/or protein transport may be impaired leading to abnormalities in endosomal function (18). If so, then the increase in lysosomes may be a marker of neuronal dysfunction before neurodegeneration, and as such, the *Atm*−/− mice may be a good model for the study of early defects that ultimately cause neuronal death in A-T.

Finally, two recent reports suggest that A-T may share defects common to other neurodegenerative diseases. Analysis of the midbrain of *Atm*−/− mice showed decreased numbers of tyrosine-hydroxylase-positive neurons in the substantia nigra and ventral tegmental area (25). In addition, *Atm*−/−

Table 1. Lysososomal counts

Animal	No. PC	S, μm² per PC	No. LY	LY I	LY II	LY (I + II)	LY lipo	MVB	No. LY/PC	No. LY per μm²
Wt 1	11	88	35	8	13	21	14	22	3.18	0.036
Wt 2	11	91	30	6	16	22	8	12	2.73	0.03
Wt 3	11	90	38	11	13	24	14	18	3.45	0.038
Wt 4	11	93	43	26	9	35	8	23	3.9	0.042
Wt 5	11	100	44	20	13	33	11	26	4	0.04
Total	**55**	**92.4**	**190**	**71**	**64**	**135**	**55**	**101**	**3.45**	**0.037**
Atm−/− 1	11	87	68	27	27	54	16	22	6.18	0.071
Atm−/− 2	11	96	79	39	24	63	16	37	7.18	0.075
Atm−/− 3	11	95	60	29	15	44	17	24	5.45	0.057
Atm−/− 4	11	93	62	26	17	43	19	10	5.64	0.061
Atm−/− 5	11	88	63	27	22	49	14	15	5.73	0.065
Total	**55**	**91.8**	**332**	**148***	**105**	**253***	**82***	**108**	**6.04****	**0.066**

S, surface area; LY, total lysosomes; LY I, primary lysosomes; LY II, secondary lysosomes; LY lipo, lipofuschin-containing lysosomes; MVB, multivesicular bodies; Wt, wild type. *, $P < 0.01$; **, $P < 0.001$.

mice show evidence of free-radical-induced oxidative damage in the brain (26). These findings, in conjunction with our findings of lysosomal accumulation in neurons of *Atm*−/− mice, suggest that A-T may share common pathways leading to neurodegeneration and cell loss as found in more common forms of neurodegenerative disease such as Alzheimer's disease and Parkinson's disease. As such, the *Atm*−/− mice may provide a useful model to study the early events common to multiple forms of neurodegeneration.

We acknowledge Jean-Claude Barthe for EM photography as well as Chidid Ezuma-Ngwu and Sununda Sadandanan for mAb production. This work was supported by grants from the A-T Children's Project and the National Ataxia Foundation (to K.D.B.), by a fellowship from the Massachusetts Biomedical Research Corporation (to E.A.H.), by National Institute of Neurological Disorders and Stroke Grants NS20591 and NS18381 (to K.H.), and by National Institutes of Health Grant 5R25 RR10836-02 to The Salk Institute for Biological Studies (to A.J.P.). C.B. is supported by the Frederick B. Rentschler Development Chair and a grant from the A-T Children's Project.

1. Brown, K. D., Ziv, Y., Sadanandan, S. N., Chessa, L., Collins, F. S., Shiloh, Y. & Tagle, D. A. (1997) *Proc. Natl. Acad. Sci. USA* **94,** 1840–1845.
2. Lakin, N. D., Weber, P., Stankovic, T., Rottinghaus, S. T., Taylor, A. M. & Jackson, S. P. (1996) *Oncogene* **13**, 2707–2716.
3. Watters, D., Khanna, K. K., Beamish, H., Birrell, G., Spring, K., Kedar, P., Gatei, M., Stenzel, D., Hobson, K., Kozlov, S., *et al*. (1997) *Oncogene* **14,** 1911–1921.
4. Rotman, G. & Shiloh, Y. (1998) *Hum. Mol. Genet*. **7,** 1555–1563.
5. Brown, K., Barlow, C. & Wynshaw-Boris, A. (1999) *Am. J. Hum. Genet*. **64,** 46–50.
6. Barlow, C., Hirotsune, S., Paylor, R., Liyanage, M., Eckhaus, M., Collins, F., Shiloh, Y., Crawley, J. N., Ried, T., Tagle, D., *et al*. (1996) *Cell* **86,** 159–171.
7. Elson, A., Wang, Y., Daugherty, C. J., Morton, C. C., Zhou, F., Campos-Torres, J. & Leder, P. (1996) *Proc. Natl. Acad. Sci. USA* **93,** 13084–13089.
8. Herzog, K. H., Chong, M. J., Kapsetaki, M., Morgan, J. I. & McKinnon, P. J. (1998) *Science* **280,** 1089–1091.
9. Xu, Y., Ashley, T., Brainerd, E. E., Bronson, R. T., Meyn, M. S. & Baltimore, D. (1996) *Genes Dev.* **10,** 2411–2422.
10. Kuljis, R., Xu, Y., Aguila, M. & Baltimore, D. (1997) *Proc. Natl. Acad. Sci. USA* **94,** 12688–12693.
11. Harlow, E. & Lane, D. (1988) *Antibodies: A Laboratory Manual* (Cold Spring Harbor Lab. Press, Plainview, NY).
12. Gately, D., Hittle, J., Chan, G. & Yen, T. (1998) *Mol. Biol. Cell* **9,** 2361–2374.
13. Herrup, K. & Sunter, K. (1986) *Dev. Biol.* **117,** 417–427.
14. Soares, H., Morgan, J. & McKinnon, P. (1998) *Neuroscience* **86,** 1045–1054.
15. Oka, A. & Takashima, S. (1998) *Neurosci. Lett.* **252,** 195–198.
16. Burd, C., Babst, M. & Emr, S. (1998) *Semin. Cell Dev. Biol.* **9,** 527–533.
17. Barlow, C., Liyanage, M., Moens, P. B., Tarsounas, M., Nagashima, K., Brown, K., Rottinghaus, S., Jackson, S. P., Tagle, D., Ried, T., *et al*. (1998) *Development (Cambridge, U.K.)* **125,** 4007–4017.
18. Lim, D. S., Kirsch, D. G., Canman, C. E., Ahn, J. H., Ziv, Y., Newman, L. S., Darnell, R. B., Shiloh, Y. & Kastan, M. B. (1998) *Proc. Natl. Acad. Sci. USA* **95,** 10146–10151.
19. Hendry, I. (1976) *Neurocytology* **5,** 337–349.
20. Mayer, R., Laszlo, L., Landon, M., Hope, J. & Lowe, J. (1992) *Ann. N.Y. Acad. Sci.* **674,** 149–160.
21. Nixon, R. A. & Cataldo, A. M. (1993) *Ann. N.Y. Acad. Sci.* **28,** 87–109.
22. Nixon, R. & Cataldo, A. (1995) *Trends Neurosci.* **18,** 489–496.
23. Mayer, R. J., Tipler, C., Arnold, J., Laszlo, L., Al-Khedhairy, A., Lowe, J. & Landon, M. (1996) *Adv. Exp. Med. Biol.* **389,** 261–269.
24. Bernstein, H. G., Kirschke, H., Wiederanders, B., Pollak, K. H., Zipress, A. & Rinne, A. (1996) *Mol. Chem. Neuropathol.* **27,** 225–247.
25. Eilam, R., Peter, Y., Elson, A., Rotman, G., Shiloh, Y., Groner, Y. & Segal, M. (1998) *Proc. Natl. Acad. Sci. USA* **95,** 12653–12656.
26. Barlow, C., Dennery, P. A., Shigenaga, M. K., Smith, M. A., Morrow, J. D., Roberts, L. J., II, Wynshaw-Boris, A. & Levine, R. L. (1999) *Proc. Natl. Acad. Sci. USA* **96,** 9915–9919.